Research Article | Vol. 26, No. 20 | 1 Oct 2018 | OPTICS EXPRESS 26205
Optics EXPRESS

Near-infrared acetylene sensor system using off-axis integrated-cavity output spectroscopy and two measurement schemes

KAIYUAN ZHENG,[1] CHUANTAO ZHENG,[1,*] QIXIN HE,[1] DAN YAO,[1] LIEN HU,[1] YU ZHANG,[1] YIDING WANG,[1] AND FRANK K. TITTEL[2]

[1]*State Key Laboratory of Integrated Optoelectronics, College of Electronic Science and Engineering, Jilin University, 2699 Qianjin Street, Changchun 130012, China*
[2]*Department of Electrical and Computer Engineering, Rice University, 6100 Main Street, Houston, TX 77005, USA*
**zhengchuantao@jlu.edu.cn*

Abstract: For highly sensitive and accurate acetylene (C_2H_2) detection, a near-infrared (NIR) off-axis integrated-cavity output spectroscopy (OA-ICOS) sensor system based on an ultra-compact cage-based absorption cell was proposed. The absorption cell with dimensions of 10 cm × 8 cm × 6 cm realized a dense-pattern and an easily-aligned stable optical system. The OA-ICOS sensor system employed a 6cm-long optical cavity that was formed by two mirrors with a reflectivity of 99.35% and provided an effective absorption path length of ~9.28 m. The performance of the C_2H_2 sensor system based on two measurement schemes, i.e. laser direct absorption spectroscopy (LDAS) and wavelength modulation spectroscopy (WMS) is reported. A NIR distributed feedback (DFB) laser was employed for targeting a C_2H_2 absorption line at 6523.88 cm^{-1}. An Allan deviation analysis yielded a detection sensitivity of 760 parts-per-billion in volume (ppbv) for an averaging time of 304 s using the LDAS-based OA-ICOS. A detection sensitivity of 85 ppbv for an averaging time of 250 s was obtained using the WMS-based OA-ICOS, which was further improved by a factor of ~9 compared to the result obtained with the LDAS method. The proposed sensor system has the advantages of reduced size and cost with acceptable detection sensitivity, which is suitable for applications in trace gas sensing in harsh environments and weight-limited balloon-embedded observations.

OCIS codes: (280.3420) Laser sensors; (300.6340) Spectroscopy, infrared; (140.5965) Semiconductor lasers, quantum cascade.

References

1. J. S. Li, G. Durry, J. Cousin, L. Joly, B. Parvitte, and V. Zeninari, "Self-broadening coefficients and positions of acetylene around 1.533 μm studied by high-resolution diode laser absorption spectrometry," J. Quant. Spectrosc. Radiat. Transf. **111**(15), 2332–2340 (2010).
2. Y. Cao, W. Jin, H. L. Ho, L. Qi, and Y. H. Yang, "Acetylene detection based on diode laser QEPAS: combined wavelength and residual amplitude modulation," Appl. Phys. B **109**(2), 359–366 (2012).
3. K. C. Utsav, E. F. Nasir, and A. Farooq, "A mid-infrared absorption diagnostic for acetylene detection," Appl. Phys. B **120**(2), 223–232 (2015).
4. G. M. Ma, S. J. Zhao, J. Jiang, H. T. Song, C. R. Li, Y. T. Luo, and H. Wu, "Tracing acetylene dissolved in transformer oil by tunable diode laser absorption spectrum," Sci. Rep. **7**(1), 14961 (2017).
5. Q. X. He, C. T. Zheng, H. F. Liu, B. Li, Y. D. Wang, and F. K. Tittel, "Performance improvement of a near-infrared acetylene sensor system by reducing residual amplitude modulation," Laser Phys. **27**(5), 055702 (2017).
6. P. Malara, P. Maddaloni, G. Gagliardi, and P. De Natale, "Combining a difference-frequency source with an off-axis high-finesse cavity for trace-gas monitoring around 3 microm," Opt. Express **14**(3), 1304–1313 (2006).
7. L. Richard, I. Ventrillard, G. Chau, K. Jaulin, E. Kerstel, and D. Romanini, "Optical-feedback cavity-enhanced absorption spectroscopy with an interband cascade laser: application to SO_2 trace analysis," Appl. Phys. B **122**(9), 247–254 (2016).
8. M. Gianella and G. A. D. Ritchie, "Cavity-enhanced near-Infrared laser absorption spectrometer for the measurement of acetonitrile in breath," Anal. Chem. **87**(13), 6881–6889 (2015).
9. J. Morville, S. Kassi, M. Chenevier, and D. Romanini, "Fast, low-noise, mode-by-mode, cavity-enhanced absorption spectroscopy by diode-laser self-locking," Appl. Phys. B **80**(8), 1027–1038 (2005).

#340473 https://doi.org/10.1364/OE.26.026205
Journal © 2018 Received 24 Jul 2018; revised 10 Sep 2018; accepted 11 Sep 2018; published 21 Sep 2018

Optics EXPRESS

10. D. Romanini, M. Chenevier, S. Kassi, M. Schmidt, C. Valant, M. Ramonet, J. Lopez, and H. Jost, "Optical-feedback cavity-enhanced absorption: a compact spectrometer for real-time measurement of atmospheric methane," Appl. Phys. B **83**(4), 659–667 (2006).
11. G. Kowzan, K. F. Lee, M. Paradowska, M. Borkowski, P. Ablewski, S. Wójtewicz, K. Stec, D. Lisak, M. E. Fermann, R. S. Trawiński, and P. Masłowski, "Self-referenced, accurate and sensitive optical frequency comb spectroscopy with a virtually imaged phased array spectrometer," Opt. Lett. **41**(5), 974–977 (2016).
12. M. Abe, K. Iwakuni, S. Okubo, and H. Sasada, "Design of cavity-enhanced absorption cell for reducing transit-time broadening," Opt. Lett. **39**(18), 5277–5280 (2014).
13. M. Nations, S. Wang, C. S. Goldenstein, K. Sun, D. F. Davidson, J. B. Jeffries, and R. K. Hanson, "Shock-tube measurements of excited oxygen atoms using cavity-enhanced absorption spectroscopy," Appl. Opt. **54**(29), 8766–8775 (2015).
14. V. L. Kasyutich, C. E. Canosa-Mas, C. Pfrang, S. Vaughan, and R. P. Wayne, "Off-axis continuous-wave cavity-enhanced absorption spectroscopy of narrow-band and broadband absorbers using red diode lasers," Appl. Phys. B **75**(6–7), 755–761 (2002).
15. J. B. Leen, X. Y. Yu, M. Gupta, D. S. Baer, J. M. Hubbe, C. D. Kluzek, J. M. Tomlinson, and M. R. Hubbell 2nd, "Fast in situ airborne measurement of ammonia using a mid-infrared off-axis ICOS spectrometer," Environ. Sci. Technol. **47**(18), 10446–10453 (2013).
16. J. B. Paul, L. Lapson, and J. G. Anderson, "Ultrasensitive absorption spectroscopy with a high-finesse optical cavity and off-axis alignment," Appl. Opt. **40**(27), 4904–4910 (2001).
17. D. S. Baer, J. B. Paul, M. Gupta, and A. O'Keefe, "Sensitive absorption measurements in the near-infrared region using off-axis integrated-cavity-output spectroscopy," Appl. Phys. B **75**(2–3), 261–265 (2002).
18. W. Zhao, X. Gao, W. Chen, W. Zhang, T. Huang, T. Wu, and H. Cha, "Wavelength modulated off-axis integrated cavity output spectroscopy in the near infrared," Appl. Phys. B **86**(2), 353–359 (2007).
19. R. Centeno, J. Mandon, S. M. Cristescu, and F. J. M. Harren, "Three mirror off axis integrated cavity output spectroscopy for the detection of ethylene using a quantum cascade laser," Sens. Actuators B Chem. **203**(21), 311–319 (2014).
20. http://www.spectraplot.com/absorption
21. D. Rehle, D. Leleux, M. Erdelyi, F. Tittel, M. Fraser, and S. Friedfeld, "Ambient formaldehyde detection with a laser spectrometer based on difference-frequency generation in PPLN," Appl. Phys. B **72**(8), 947–952 (2001).
22. K. Liu, T. Liu, J. Jiang, G. D. Peng, H. Zhang, D. Jia, Y. Wang, W. Jing, and Y. Zhang, "Investigation of wavelength modulation and wavelength sweep techniques in intracavity fiber laser for gas detection," J. Lightwave Technol. **29**(1), 15–21 (2011).
23. W. Ye, C. Li, C. Zheng, N. P. Sanchez, A. K. Gluszek, A. J. Hudzikowski, L. Dong, R. J. Griffin, and F. K. Tittel, "Mid-infrared dual-gas sensor for simultaneous detection of methane and ethane using a single continuous-wave interband cascade laser," Opt. Express **24**(15), 16973–16985 (2016).

1. Introduction

Acetylene (C_2H_2) is colorless, inflammable and explosive at ambient temperatures and pressure and is widely used as a fuel and a basic raw material in organic synthesis in the industrial applications. Therefore, accurate measurements and monitoring of C_2H_2 in the industrial field is extremely important to ensure high quality of petrochemical materials and products [1–4]. To achieve a high detection sensitivity, a high-finesse cavity based absorption spectroscopy technique can be used for increasing the effective absorption path length while retaining a relatively small sample volume [5,6]. In particular, cavity ring-down spectroscopy (CRDS) [7,8], cavity-enhanced absorption spectroscopy (CEAS) [9–13] and off-axis integrated-cavity output spectroscopy (OA-ICOS) [14,15] are effective spectroscopic techniques developed in the past decade and allow a considerable improvement in detection sensitivity. These techniques offer different advantages and disadvantages in terms of selectivity, portability, sensitivity and cost.

Among these techniques for high sensitive measurements, OA-ICOS offers robustness, low maintenance, simple operation as well as a real-time monitoring capability. For these reasons this technique becomes widely used in trace gas sensing. In 2001, Paul et al. [16] reported the first OA-ICOS set-up using a single-mode continuous-wave laser for the detection of molecular oxygen (O_2). A noise equivalent absorption sensitivity (NEAS) of 1.8×10^{-10} cm^{-1} $Hz^{-1/2}$ was observed in a 10 s averaging time. In 2002, a DFB diode laser-based OA-ICOS instrument was reported for sensitive CO measurements. A minimum detectable absorption of 3.1×10^{-11} cm^{-1} $Hz^{-1/2}$ for an effective optical path of 4.2 km was obtained in a 50 s integration time [17]. In 2007, an improved OA-ICOS instrument in conjunction with a WMS technique was developed using a DFB diode laser for CO_2 detection. A minimum

Optics EXPRESS

detectable absorption of 3.6 ppmv $Hz^{-1/2}$ was achieved [18]. Recently, new methods have been reported to improve the OA-ICOS performance. Centeno et al. [19] added another highly-reflective mirror with a small entrance hole in front of the cavity to re-inject the reflected light into the cavity, enhancing the detection sensitivity of the system by a factor of 4. A detection limit of 2.5 ppbv was achieved for ethylene (C_2H_4) detection in a 2 min averaging time, which is equal to a NEAS of 2.5×10^{-9} cm^{-1} $Hz^{-1/2}$.

In order to achieve a longer absorption path, most of the reported OA-ICOS systems possess a relatively long (~50–100 cm) cavity length. However, a long cavity is not necessarily conductive to system integration and collimation of the beam within the cavity. In this paper, a small cavity with a short length of only 6 cm was implemented and a cage-based absorption cell was fabricated for realizing a more compact and simpler alignment of the OA-ICOS sensor system. C_2H_2 detection experiments were carried out to validate the sensor performance. A DFB laser emitting at 1.532 μm was selected for targeting a C_2H_2 absorption line at 6523.88 cm^{-1}. A LabVIEW-based data-processing system was developed, which consists of a scan and modulation signal generator, a signal acquisition module and a lock-in amplifier. Furthermore, two measurement schemes, LDAS and WMS, were applied to OA-ICOS respectively and a performance comparison was made between these two methods. Such a sensor system can perform the normal operation of driving a DFB laser as well as extracting the C_2H_2 harmonic signal from the absorption spectrum employing a laptop and a data acquisition (DAQ) card, which can be made in a compact and inexpensive package for sensitive trace gas measurements in harsh environments.

2. Sensor configuration

2.1. OA-ICOS sensor architecture

The architecture of the OA-ICOS is depicted in Fig. 1, which includes an electrical, an optical and a gas sampling system. The electrical part of the sensor system consists of a laptop, a DAQ card (Model USB-6211, National Instrument, USA), a laser current driver (LDC-3724B, ILX Lightwave, USA) and a temperature controller (TED200C, Thorlabs, USA). The temperature of the DFB laser was set to 13.3 °C. A scan signal (2 Hz triangular-wave) was generated by the LabVIEW controlled DAQ card to drive the DFB laser. A WMS technique was used for C_2H_2 detection, which requires a scan and modulation signal (2 Hz triangular-wave plus a 3 kHz sine-wave) to drive the DFB laser. Furthermore, the signal from the detector (PDA10CS, Thorlabs, USA) was sent to the DAQ for data acquisition triggered by the signal generation module.

In the optical part, the light source used was a DFB diode laser (Corning Lasertron, USA) operating in the NIR at 1.532 μm. An optical isolator (IO-H-1550APC, Thorlabs, USA) was placed in front of the laser source to minimize the optical feedback from the cavity to the laser. A collimator (50-1550A-APC, Thorlabs, USA) was used to align the beam, and a round beam shape with a diameter of ~0.5 mm was obtained. The visible beam from the alignment laser (λ = 632.8 nm) were aligned collinearly with the DFB beam by means of a flip mirror (Newport, USA) as a guide beam to assist in the optical alignment of the sensor system. The combined beam was coupled into a high-finesse cavity using two plane mirrors of M1 and M2. The two mirrors were used to adjust the angle of the incidence beam for achieving a good coupling of the laser into the cavity. The optical cavity was 6 cm long consisting of two reflective mirrors (99.35% @ 1450-1670 nm, Layertec GmbH, Germany) with a radius of curvature of 20 cm. With a selected cavity length of 6 cm, more high-order modes were excited in the cavity, the free spectral range (FSR) decreased, and the optical noise became relative smaller. This results in a good cavity mode stability, an improved effective optical path length with a large transmission signal from the detector. The output of the cavity was collected by an achromatic lens (f = 6 cm) and focused on the InGaAs amplified detector.

Optics EXPRESS

In the gas sampling system, nitrogen (N_2) was used as the balance gas to mix with a 1000 ppmv C_2H_2 gas to obtain C_2H_2 samples with different concentration levels via a gas mixing system (Series 4000, Environics, USA).

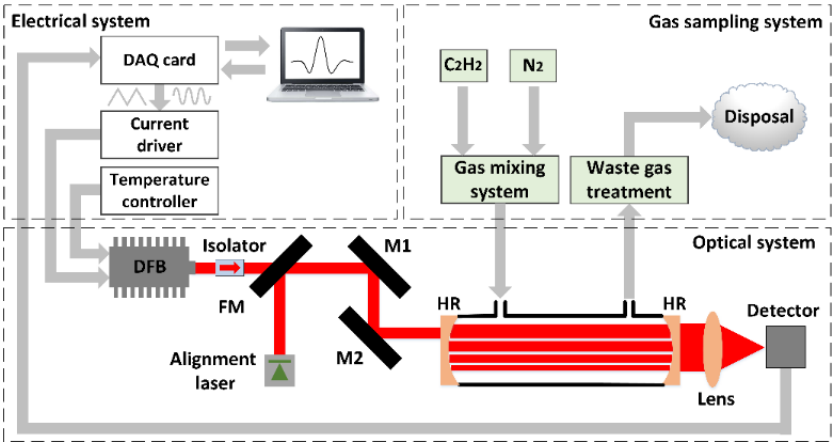

Fig. 1. Experimental setup of the OA-ICOS set-up, including an electrical system, an optical system as well as a gas sampling system. DFB: distributed feedback laser; FM: flip mirror; M1and M2: plane mirror; HR: highly-reflective mirror.

2.2. Cage-based absorption cell architecture

The computer aided design (CAD) image of the cage-based absorption cell is depicted in Fig. 2(a). The dimensions and mass of the cell are 10 × 8 × 6 cm^3 and 1 kg, respectively. The cage system with a cavity length of 6 cm consists of cage plates and cage rods, as shown in Fig. 2(b). The cage plates served as basic building blocks for the cage system. C1, C3 and C5 were used to form the cage structure and ensure its stability. C2 and C4 were used to install the highly-reflective mirrors separated by a distance of 6 cm. The cage rod was used to connect cage plates and optical mounts in the cage system. A tilted window (WG10530-C, Thorlabs, USA) combined with a customized flange plate was placed on both sides of the cell to avoid interference fringes. The center position of the window should coincide with the center position of the cage plate to ensure alignment of the light path. A gas inlet (H1) and outlet (not shown in Fig. 2a) were located in front and in the rear of the cell, respectively. A sealing ring was placed on top of the cell. Moreover, the absorption cell can be sealed when the sealing ring is squeezed to deform as a result of the pressure from the lid (not shown in Fig. 2a). Figure 2(c) shows the photograph of the fabricated and sealed absorption cell. This kind of cell has the advantages of dense mode pattern, easy and fast alignment, good stability, strong shock resistance and robustness. In addition, the cavity length can be easily adjusted without affecting/worsening the collimation performances. Besides, in order to maintain the mirror reflectivity, Teflon polytetrafluoroethylene (PTFE) filter can be used in the gas inlet to remove ambient impurities and aerosols, and a frequent change of the filter is needed. Also, a small purge flow of zero air or N_2 can be injected to both sides of the cavity to keep the highly-reflective mirrors clean.

Optics EXPRESS

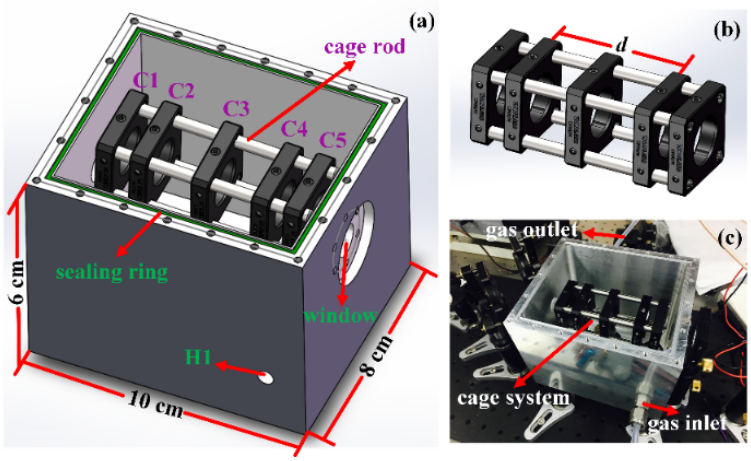

Fig. 2. (a) CAD image of the cage-based absorption cell with dimensions of length (10 cm), width (8 cm) and height (6 cm). (b) CAD image of the cage system with a cavity length of d = 6 cm. (c) Photograph of the fabricated absorption gas cell.

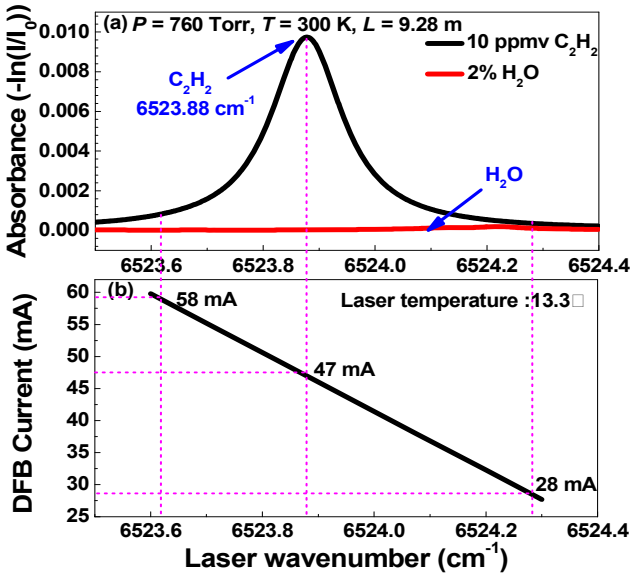

Fig. 3. (a) HITRAN based absorption spectra of C_2H_2 (10 ppmv) and H_2O (2%) in a spectral range from 6523.5 to 6524.4 cm^{-1} at a pressure of 760 Torr and an absorption length of 9.28 m. C_2H_2 and H_2O lines are shown in black and red, respectively. (b) Curves of the DFB laser emission wavenumber as a function of the laser drive current at 13.3 °C.

3. Results and discussion

3.1. C_2H_2 line selection

The C_2H_2 molecule has an overtone vibrational band near 1.53 μm. At this wavelength, the potential spectral interference originates mainly from water (H_2O). HITRAN (high- resolution transmission molecular absorption database) absorption spectra of 10 ppmv C_2H_2 and 2% H_2O in the spectral region from 6523.5 to 6524.4 cm^{-1} are depicted in Fig. 3(a). The simulated conditions were at a gas pressure of 760 Torr, a temperature of 300 K and an effective optical path length of 9.28 m. An interference-free C_2H_2 absorption line centered at 1532.8 nm (6523.88 cm^{-1}) was selected as the optimum target line. Figure 3(b) shows relation

Optics EXPRESS

curve of the DFB laser emission wavenumber versus the laser drive current at an operating temperature of 13.3 °C. To target the 6523.88 cm^{-1} C_2H_2 absorption line, the scan range of the driving current was set to 28–58 mA, corresponding to a wavenumber range of 6523.6–6524.3 cm^{-1}. Based on Fig. 3(a), the half width at the half-maximum (HWHM) of the absorption line is 0.062 cm^{-1}.

3.2. LDAS-based OA-ICOS sensor performances

For targeting the C_2H_2 absorption line at 6523.88 cm^{-1}, the DFB laser was operated at a current of 47 mA and a temperature of 13.3 °C, which provided an optical power of ~2 mW. The scan signal was a trigonometric signal with a frequency of 2 Hz. A peak-to-peak amplitude of 1.5V yielded a DFB laser current scan from 28 mA to 58 mA (20 mA/V). The sampling rate of the LabVIEW-based DAQ card was set to 100 kHz, resulting in 50000 data points per triangular period. Sync sampling was realized by using the scan signal of the laser as the triggering signal. The sampling time plus the data processing time is ~2 s to obtain an absorption signal.

A driving current increasing linearly from 28 mA to 58 mA was applied to the laser to scan the selected C_2H_2 absorption line, as shown in Fig. 4(a). The measured cavity transmission power and the output voltage from the detector are shown in Fig. 4(a), where the cell was filled with pure N_2. It can be seen that both the cavity transmission power and the output voltage changes linearly with the scan time, which indicates that the output voltage also changes linearly with the cavity transmission power. A typical C_2H_2 absorption signal acquired from a known concentration level of 550 ppmv is depicted in Fig. 4(b) together with a fitted baseline. In order to obtain the baseline, the absorption peak was removed from the absorption spectrum. Next, the remaining data points were fitted by means of a fifth order polynomial. The maximum absorption voltage of the detector's response (V_1) was 0.03012 V. The red line was the fitted background signal. The non-absorption voltage (V_2) on the red line was 0.04881 V. The absorbance (A) can be calculated from Eq. (1)

$$A = -\ln(V_1 / V_2) \tag{1}$$

Therefore, the absorbance was determined to be 0.48, corresponding to a light path of 9.28 m as compared to the simulation result on the SpectraPlot website [20]. Since the effective optical path of OA-ICOS is expressed as $L = d/(1-R)$, the calibrated mirror reflectivity of R is therefore calculated as 99.35% with a cavity length d of 6 cm, which is consistent with the theoretical value. The absorption coefficient (α) as a function of time was calculated, as shown in Fig. 4(c). A Voigt line shape was fitted to the absorbance to retrieve the target gas concentration [21]. A C_2H_2 concentration value of 549 ppm was obtained, which is consistent with the actual concentration level. Residual between the absorption spectrum and Voigt fitting line is shown in Fig. 4(d). In this manner, with a fit residual of 6.4×10^{-6} cm^{-1} and a peak absorption of 5.8×10^{-4} cm^{-1}, a signal to noise ratio (SNR) of 90 was obtained.

Optics EXPRESS

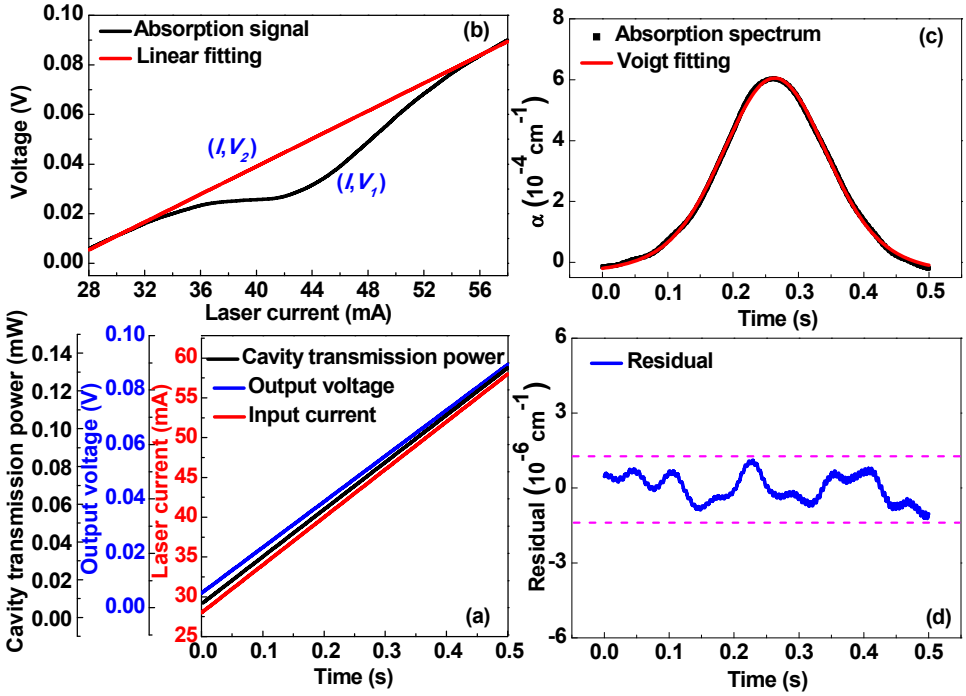

Fig. 4. (a) Curves of the cavity transmission light power, the output voltage from the detector and the laser current versus scan time within one period. (b) C_2H_2 absorption spectrum around 6523.88 cm^{-1} (black line) with a fitted baseline (red line). (c) Calculated absorbance as a function of scan time with a Voigt line shape fitting based on figure (a). (d) Residual between the absorbance line and the fitted Voigt line based on figure (b).

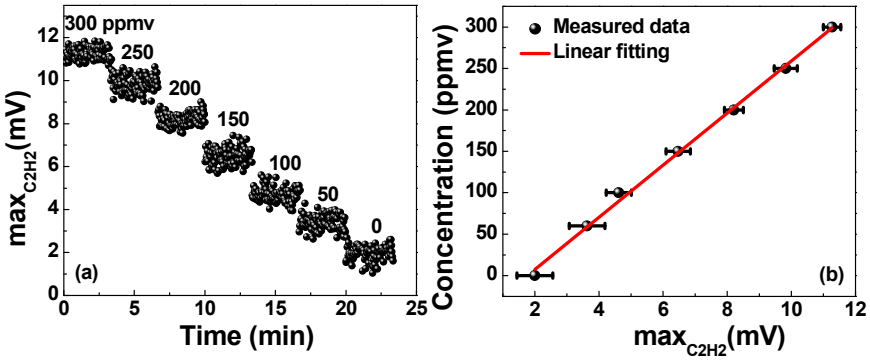

Fig. 5. (a) Measured max_{C2H2} versus calibration time for different C_2H_2 concentration levels ranging from 0 to 300 ppmv. (b) Experimental data and fitting curve of C_2H_2 concentration versus max_{C2H2}.

3.2.1. Calibration and data-fitting

In order to calibrate the sensor, the C_2H_2 gas samples in the range of 0 to 300 ppmv in steps of 50 ppmv were prepared using the gas mixing system. The amplitude of the absorption signal was recorded for ~3 min with no averaging for each C_2H_2 concentration level, as shown in Fig. 5(a). The measured amplitude for each concentration was averaged and plotted as a function of C_2H_2 concentration, as shown in Fig. 5(b). A linear relation (R-square value: 0.9967) was observed between the amplitude of the absorption signal ($max_{C_2H_2}$, in mV) and the C_2H_2 concentration (C, in ppmv), expressed as

$$C = 31.427 \times \max_{C_2H_2} - 55.226 \quad (2)$$

3.2.2. Sensor stability

In order to obtain the detection limit of the LDAS-based OA-ICOS sensor system, the noise level was determined by passing pure N_2 into the gas cell and subsequent monitoring of the detected maximal absorption amplitude. The amplitude was transformed to a C_2H_2 concentration based on the relationship of Eq. (2). As shown in Fig. 6(a), the measurements of the C_2H_2 sample with zero concentration were performed over a time period of ~1 h with a sampling interval of ~2 s. The total variation range of the measured concentration is from ~30 to 40 ppmv for a 1 h measurement time. An Allan-Werle analysis was utilized to assess the stability of the C_2H_2 sensor system. As shown in Fig. 6(b), the Allan deviation was plotted on a log-log scale versus the averaging time, which indicates a measurement precision of 11 ppmv with an averaging time of 2 s. Furthermore, a detection limit of 760 ppbv was obtained with a 304 s averaging time.

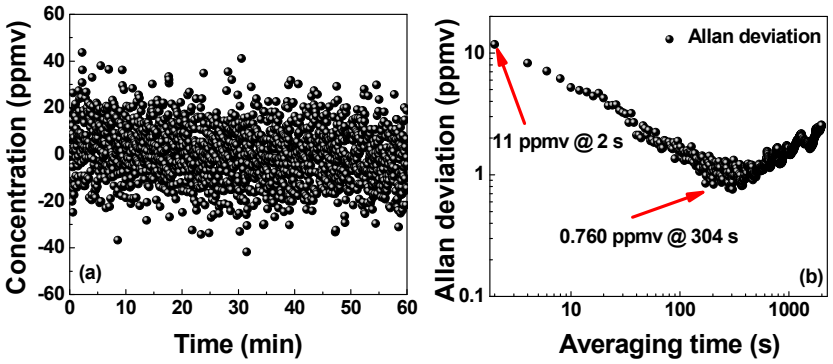

Fig. 6. (a) C_2H_2 concentration measurements of the sample with zero concentration for a time period of ~1 hour. (b) Allan deviation plot as a function of averaging time, based on the data shown in Fig. 6(a).

For the calibration data set, the standard deviation of the 3min's concentration measurements on a 50 ppm sample in Fig. 5(a) is ~10.7 ppmv, which is nearly the same as the Allan deviation value (11 ppmv) obtain from Fig. 6(b). Based on Figs. 4(c) and 4(d), the detection limit estimated from the Voigt fit residual is approximately 550/90 = 6.1 ppmv. The difference is probably caused by optical noise, including cavity mode noise caused by mechanical vibration and instability of the laser power in long-term tests. The optical noise may have some impact on the quality of the measurement, but we can minimize such effect by eliminating the background signal, reducing the mechanical vibration, and averaging the spectral signals.

3.3. WMS-based OA-ICOS sensor performances

In the WMS scheme, data sampling and processing were realized on a LabVIEW-based platform. The DAQ card with a resolution of 16 bits and a maximum sampling rate of 250 ksps was used for signal acquisition and then the obtained signal was sent to the LabVIEW-based lock-in amplifier for 2*f* signal extraction. Detailed structure of the lock-in amplifier can be found in [23]. The sampling rate of the DAQ card was set to 100 kHz. The low-pass filter is a key module of the lock-in amplifier, which has three main parameters, i.e. filter type, filter order and cut-off frequency. There are two types of low-pass filters available, i.e. Butterworth and Chebyshev. The Butterworth type is preferred due to a more stable amplitude-frequency characteristic in the passband. A higher order filter is more helpful in denoising but causes a larger delay. The cut-off frequency mainly influences the smoothness

Optics EXPRESS

of the 2*f* signal waveform. In this work, through optimization, the used low-pass filter is a second-order Butterworth filter with a cut-off frequency of 20 Hz.

3.3.1. Modulation depth optimization

In order to improve the detection sensitivity, wavelength modulation and second harmonic (2*f*) detection was applied to the C_2H_2 sensor system. In WMS, an appropriate selection of the modulation amplitude is required to maximize the 2*f* signal amplitude. The optimized modulation depth is 2.2 times of the HWHM of the absorption line [22,23]. In this work, the modulation depth was experimentally optimized for a gas pressure of 760 Torr. The measured amplitude of the 2*f* signal for a 350 ppmv C_2H_2 sample at different modulation amplitude were recorded, as depicted in Fig. 7. The maximum 2*f* signal amplitude of C_2H_2 is achieved at a modulation depth of 0.13 cm^{-1} and an amplitude of ~0.3 V. Thus a modulation amplitude of 0.3 V was selected for the sensor system, leading to a modulation coefficient of 2.1.

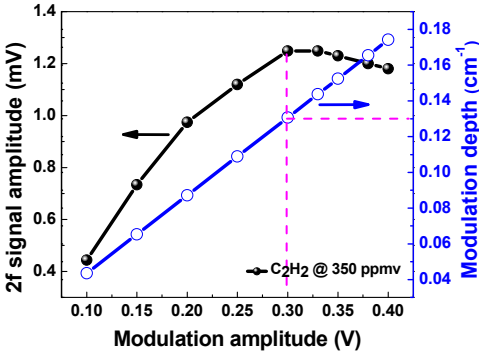

Fig. 7. Measured amplitude of the 2*f* signal and the modulation depth as a function of modulation amplitude of the sinewave signal.

3.3.2. Calibration and data-fitting

For targeting the C_2H_2 absorption line at 6523.88 cm^{-1}, the DFB laser was operated at a temperature of 13.3 °C. The scan signal was a triangular ramp with a frequency of 2 Hz and an amplitude of 1.3 V. The sine-wave modulation signal possessed a frequency of 3 kHz and an amplitude of 0.3 V. The sampling time plus the data processing time is ~2 s to obtain a 2*f* signal. Sync sampling was realized by using the scan signal of the laser as a trigger signal.

With the optimized sensor parameters, C_2H_2 sensor calibration was carried out by using diluted standard C_2H_2 gas with nine different concentration levels in the range of 0 to 400 ppmv in a step of 50 ppmv. The maximum amplitude of the 2*f* absorption signal was recorded for ~3 min with no averaging for each C_2H_2 concentration level, as shown in Fig. 8(a). The measured amplitude for each concentration was averaged and plotted as a function of C_2H_2 concentration, as shown in Fig. 8(b). A linear relation (R-square value: 0.9983) was observed between the 2*f* signal amplitude (max(2*f*), in mV) and the concentration (*C*, in ppmv), expressed as

$$C = 317.482 \times \max(2f) - 30.723 \quad (3)$$

Optics EXPRESS

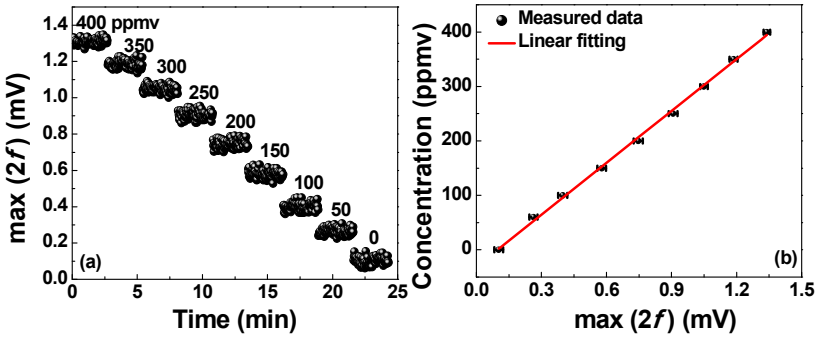

Fig. 8. (a) Measured 2*f* amplitude, max(2*f*), versus calibration time for different C_2H_2 concentration levels ranging from 0 to 400 ppmv. (b) Experimental data and fitting curve of the C_2H_2 concentration versus max (2*f*).

3.3.3. Sensor stability

In order to obtain the detection limit of the WMS-based OA-ICOS sensor system, the noise level was determined by passing pure N_2 into the gas cell and subsequent monitoring of the detected maximal absorption amplitude. The amplitude was transformed to C_2H_2 concentration based on the relationship of Eq. (3). As shown in Fig. 9(a), the entire measurements of the C_2H_2 sample with zero concentration were performed over a time period of ~1 h with a sampling interval of ~2 s. The total variation range of the measured concentration is from −3 to 4 ppmv for 1 h measurement time. An Allen-Werle analysis was utilized to assess the stability of the C_2H_2 sensor. As shown in Fig. 9(b), the Allan deviation was plotted on a log-log scale versus the averaging time, which indicates a measurement precision of 1.2 ppmv with an averaging time of 2 s. Furthermore, a detection limit of 85 ppbv was obtained with a 250 s averaging time.

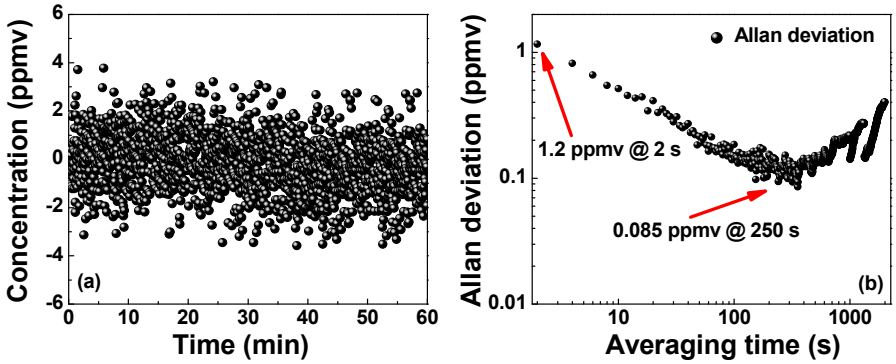

Fig. 9. (a) C_2H_2 concentration measurements of N_2 for a time period of ~1 hour. (b) Allan deviation plot as a function of averaging time, based on the data shown in Fig. 9(a).

3.3.4. SNR level estimation

A 2*f* measurement of C_2H_2 with a concentration level of 550 ppmv was performed to evaluate the performance of the developed C_2H_2 sensor system. Figure 10 shows the acquired 2*f* signal without average with a peak-to-peak amplitude of 0.00183 V. According to the calibrated curve shown in Fig. 8(b), the corresponding C_2H_2 concentration level is 550 ppmv, which is consistent with the injected C_2H_2 concentration. The noise level was determined by the standard deviation of the non-absorption wing of the 2*f* signal, which was 2.08×10^{-6} V (1σ), corresponding to a SNR of ~880 of the WMS-based sensor system.

Optics EXPRESS

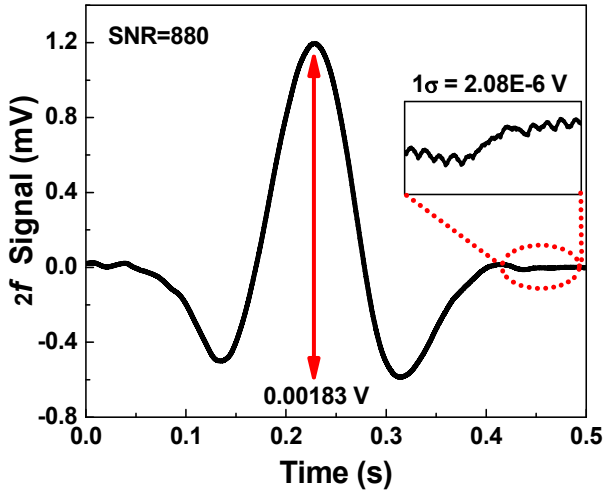

Fig. 10. The obtained 2*f* absorption spectrum of C_2H_2 at a concentration level of 550 ppmv at a pressure of 760 Torr.

3.4. Performance comparison

A performance comparison between the LDAS-based and the WMS-based OA-ICOS is implemented and demonstrated in Table 1. Using the LDAS method, the achieved SNR is 90 when the 1σ limit of detection (LoD) is 760 ppbv for a 304 s averaging time. Using the WMS method, the achieved SNR is 880 when the LoD (1σ) is 85 ppbv in a 250 s averaging time. Compared to the results obtained with LDAS under the same experimental condition, the SNR is improved by a factor of ~10 while the LoD is about 9 times better by using WMS.

Table 1. Performance comparison between the LDAS-based and WMS-based OA-ICOS sensor systems

Experimental method	SNR	LoD (1σ) (ppbv)	Averaging time (s)
LDAS	90	760	304
WMS	880	85	250

The advantage of WMS is that the obtained 2*f* signal amplitude is proportional to gas concentration, and the 1/*f* laser excess noise and baseline slope can be suppressed by selecting the optimum modulation depth. Therefore, a better SNR and LoD can be achieved, which illustrates good performances of the WMS based OA-ICOS sensor system. Further improvements in sensitivity can be made by using highly-reflective mirrors, increasing the effective mirror diameter and reducing low-frequency noise.

4. Conclusions

An OA-ICOS sensor system was developed by using a compact cage-based absorption cell. The low cost and robust cell was designed and fabricated to realize a ~9.28 m effective optical path length with a small cavity length of 6 cm, which is less sensitive to harsh environmental contamination and requires less maintenance. Experiments were carried out to obtain the performance of the sensor system using diluted C_2H_2 samples. LDAS and WMS techniques were adopted in the OA-ICOS sensor system for performance evaluation. Compared with LDAS, an enhancement factor of ~10 in SNR as well as a factor of ~9 in LoD were achieved by using WMS. A SNR of 880 and a LoD (1σ) of 85 ppbv in an averaging time of 250 s was obtained for the WMS based sensor system. The demonstrated OA-ICOS sensor system provides a compact, robust, low maintenance and cost-effective tool for trace gas sensing without decay in detection sensitivity, selectivity and reliability.

Optics EXPRESS

Funding

The National Natural Science Foundation of China (Nos. 61775079, 61627823), National Key R&D Program of China (Nos. 2017YFB0405300, 2016YFD0700101, 2016YFC0303902), Key Science and Technology R&D program of Jilin Province, China (No. 20180201046GX), Industrial Innovation Program of Jilin Province, China (No. 2017C027), and the National Science Foundation (NSF) ERC MIRTHE award and Robert Welch Foundation (No. R4925U).